ResearchGate

See discussions, stats, and author profiles for this publication at: https://www.researchgate.net/publication/6336640

Kinetic Studies of Protein Farnesyltransferase Mutants Establish Active Substrate Conformation †

ARTICLE *in* BIOCHEMISTRY · SEPTEMBER 2003

Impact Factor: 3.02 · DOI: 10.1021/bi0346852 · Source: PubMed

CITATIONS
49

READS
11

7 AUTHORS, INCLUDING:

Hua-Wen Fu
National Tsing Hua University
24 PUBLICATIONS **614** CITATIONS

SEE PROFILE

Available from: Hua-Wen Fu
Retrieved on: 23 January 2016

Kinetic Studies of Protein Farnesyltransferase Mutants Establish Active Substrate Conformation†

Jennifer S. Pickett,‡ Katherine E. Bowers,‡ Heather L. Hartman,‡ Hua-Wen Fu,§,|| Alan C. Embry,§ Patrick J. Casey,§ and Carol A. Fierke*,‡

Department of Chemistry, University of Michigan, Ann Arbor, Michigan 48109, and Department of Pharmacology and Cancer Biology, Duke University Medical Center, Durham, North Carolina 27710

Received April 29, 2003; Revised Manuscript Received June 17, 2003

ABSTRACT: The zinc metalloenzyme protein farnesyltransferase (FTase) catalyzes the transfer of a 15-carbon farnesyl moiety from farnesyl diphosphate (FPP) to a cysteine residue near the C-terminus of a protein substrate. Several crystal structures of inactive FTase·FPP·peptide complexes indicate that K164α interacts with the α-phosphate and that H248*β* and Y300*β* form hydrogen bonds with the *β*-phosphate of FPP [Strickland, C. L., et al. (1998) *Biochemistry 37,* 16601−16611]. Mutations K164Aα, H248A*β*, and Y300F*β* were prepared and analyzed by single turnover kinetics and ligand binding studies. These mutations do not significantly affect the enzyme affinity for FPP but do decrease the farnesylation rate constant by 30-, 10-, and 500-fold, respectively. These mutations have little effect on the pH and magnesium dependence of the farnesylation rate constant, demonstrating that the side chains of K164α, Y300*β*, and H248*β* do not function either as general acid−base catalysts or as magnesium ligands. Mutation of H248*β* and Y300*β*, but not K164α, decreases the farnesylation rate constant using farnesyl monophosphate (FMP). These data suggest that, contrary to the conclusions derived from analysis of the static crystal structures, the transition state for farnesylation is stabilized by interactions between the α-phosphate of the isoprenoid substrate and the side chains of Y300*β* and H248*β*. These results suggest an active substrate conformation for FTase wherein the C1 carbon of the FPP substrate moves toward the zinc-bound thiolate of the protein substrate to react, resulting in a rearrangement of the diphosphate group relative to its ground state position in the binding pocket.

Protein farnesyltransferase (FTase)[1] catalyzes the transfer of a 15-carbon isoprenoid chain from farnesyl diphosphate (FPP) onto a cysteine sulfur of protein substrates (*1*). Protein substrates of FTase contain a C-terminal CaaX motif, where C is the farnesylated cysteine and the X residue is frequently a methionine, serine, alanine, or glutamine (*2*). Farnesylation is one form of posttranslational protein lipidation; this class of modifications also includes the related geranylgeranylation, *N*-myristoylation, and *S*-acylation. Farnesylation of the protein C-terminus increases its hydrophobicity, which increases the affinity of the protein substrate for the cell membrane and is likely also important in protein−protein interactions of a number of the protein substrates (*3*−*5*). Therefore, these modifications play an important role in cell signaling by controlling localization and function of signaling molecules. Known substrates of FTase include H-Ras, K-Ras, N-Ras, RhoB, CENP-E, and CENP-F. The short-circuiting of signaling in the cell by farnesyltransferase inhibitors (FTIs) has been a tremendous area of research in the past 10 years, leading to several compounds currently in clinical trials for the treatment of human cancers (*6*, *7*).

FTase is an α/*β* heterodimer that contains an active site zinc ion that is essential for activity (*8*−*10*). The zinc ion coordinates the cysteine sulfur of the protein substrate and lowers the thiol pK_a from 8.1 to 6.4, creating a reactive thiolate at neutral pH (*11*, *12*). Available data indicate that the FTase-catalyzed reaction proceeds by an associative mechanism with dissociative character, so that, in the transition state, the C1 on FPP has carbocation character and the diphosphate leaving group develops additional negative charge (*13*, *14*).

Magnesium ions accelerate the farnesylation rate constant 700-fold (*13*). The divalent magnesium ion is proposed to coordinate with the nonbridging oxygens of the diphosphate of FPP, stabilizing the leaving group by neutralizing the

† This work was supported by National Institutes of Health Grants GM40602 (C.A.F.) and GM46372 (P.J.C.), National Institutes of Health Postdoctoral Training Grant F32 CA84757 (K.E.B.), and National Institutes of Health Training Grant GM08597 (J.S.P.).

* To whom correspondence should be addressed. E-mail: fierke@umich.edu.

‡ University of Michigan.

§ Duke University Medical Center.

|| Current address: Institute of Molecular and Cellular Biology and Department of Life Science, National Tsing Hua University, Hsinchu, Taiwan.

[1] Abbreviations: FTase, protein farnesyltransferase; FPP, farnesyl diphosphate; TCEP, tris(2-carboxyethyl)phosphine hydrochloride; Dns-GCVLS, dansylated pentapeptide Gly-Cys-Val-Leu-Ser; DTNB, 5,5′-dithiobis(2-nitrobenzoic acid); I2, FPT inhibitor II; HEPES, 4-(2-hydroxyethyl)-1-piperazineethanesulfonic acid; DTT, dithiothreitol; FPLC, fast protein liquid chromatography; SDS−PAGE, sodium dodecyl sulfate−polyacrylamide gel electrophoresis; Mes, 2-(*N*-morpholino)ethanesulfonic acid; Bes, *N*,*N*-bis(2-hydroxyethyl)-2-aminoethanesulfonic acid; Bicine, *N*,*N*-bis(2-hydroxyethyl)glycine; Heppso, *N*-(2-hydroxyethyl)piperazine-*N*′-hydroxypropanesulfonic acid; [^{3}H]-FPP, tritium-labeled farnesyl diphosphate; TLC, thin-layer chromatography; CPM, counts per minute; [^{3}H]FMP, tritium-labeled farnesyl monophosphate; FRET, fluorescence resonance energy transfer; EDTA, (ethylenedinitrilo)tetraacetic acid; RMSD, root mean square deviation.

10.1021/bi0346852 CCC: $25.00 © 2003 American Chemical Society
Published on Web 07/26/2003

negative charge and promoting the development of positive charge at C1. The magnesium affinity of FTase increases with pH with a pK_a of 7.4, presumably reflecting the deprotonation of the FPP diphosphate to enhance magnesium coordination (*15*). The crystal structure of FTase with the FPP analogue FPT inhibitor II (I2) and a K-Ras4B peptide shows a manganese ion in the diphosphate binding pocket of FTase, but the absence of a diphosphate group on the I2 analogue prevents accurate identification of the magnesium binding site (*16*). The amino acids of the diphosphate binding pocket of FTase are not the typical protein acidic residues that coordinate magnesium. Crystallographic analysis of the FTase·FPP·CVFM complex shows that residues Lys164α, His248*β*, Arg291*β*, Lys294*β*, and Tyr300*β* form a positively charged pocket with extensive hydrogen-bonding interactions with the diphosphate oxygens (*17*).

Although FTase has been well characterized by X-ray crystallography, the crystal structures of the ternary complexes (FTase·FPP·peptide analogue or FTase·FPP analogue·peptide) reflect an inactive substrate conformation where the two reacting atoms, the C1 of FPP and the cysteine sulfur of the peptide, are over 7 Å apart (*16*−*18*). A recent crystal structure of the FTase·farnesylated peptide complex reveals that the farnesyl moiety of the product undergoes a conformational twist in order to form a thioether bond with the peptide sulfur (*19*). These structural snapshots of the beginning and end points of the reaction provide a framework for biochemical and computational studies to address the structural nature of the transition state and the active conformation of the FPP substrate. Mutagenesis of the diphosphate binding pocket is a logical place to begin these studies, since none of the FTase·product crystal structures capture the position of the diphosphate moiety prior to its dissociation from the complex.

The diphosphate binding pocket of FTase consists primarily of residues Lys164α, His248*β*, Arg291*β*, Lys294*β*, and Tyr300*β*. Previous work has shown that mutation of Tyr300*β* to Phe (Y300F*β*), Lys164α to Ala (K164Aα), and His248*β* to Ala (H248A*β*) decreases the rate of chemistry (k_{chem}) 500-fold, 40-fold, and 10-fold, respectively (*20*, *21*). Tyr300*β* and Lys164α have been proposed to act as general acid−base catalysts on the basis of alterations in the pH dependence of steady-state kinetics of the mutants compared to wild-type FTase (*12*, *20*). Lys164α has also been implicated in binding the peptide CaaX motif and is the only residue from the α subunit proposed to be important for FTase catalysis (*21*).

In this study, we further investigate the catalytic function of residues in the diphosphate binding pocket. In particular, we examine the properties of the FTase active site mutants K164Aα, H248A*β*, and Y300F*β* using ligand binding studies and transient kinetics. The use of transient kinetics allows for isolation of the chemical rate constant (k_{chem}), so that the effect of pH and magnesium ion concentration on the chemical step of the reaction can be directly studied. Mutations at these sites have no effect on the magnesium dependence of the chemical step, the magnesium-dependent pK_a, nor the enzyme-bound peptide thiol pK_a, demonstrating that these side chains neither function as general acid−base catalysts of the farnesylation step nor do they coordinate the catalytic magnesium ion. However, these mutations do result in clear and differential effects on the rate constant for farnesylation using FMP as a substrate, suggesting that the hydroxyl of Tyr300*β* stabilizes the transition state by forming a hydrogen bond with the α-phosphate rather than the *β*-phosphate as observed in the crystal structures. Furthermore, the data provide compelling evidence that Lys164α does not interact with the α-phosphate, while His248*β* has a partial interaction with the α-phosphate. Together, our data indicate that FTase residues Lys164α, His248*β*, and Tyr300*β* function to both hold the FTase-bound FPP in an active conformation, where the C1 of FPP is in the correct position to facilitate the reaction with the thiolate nucleophile, and lower the energy of the transition state by stabilizing the formation of negative charge on the diphosphate leaving group.

EXPERIMENTAL PROCEDURES

Miscellaneous Methods. All assays were performed at 25 °C. All curve fitting was performed with Kaleidagraph (Synergy Software). [^{3}H]FPP was purchased from Amersham Pharmacia Biotech (Piscataway, NJ), vacuum-dried, washed with 100% methanol, and resuspended in 20 mM Heppso, pH 7.8, and 0.5 mM 3-14 zwittergent, to a final concentration of 20 μM. [^{3}H]FMP was obtained from American Radiolabeled Chemicals, Inc. (St. Louis, MO). The peptides GCVLS and dansylated-GCVLS were synthesized and HPLC purified by Bethyl Laboratories, Inc. (Montgomery, TX), and the University of Michigan Peptide Core (Ann Arbor, MI), respectively. The concentration of peptide was determined spectroscopically at 412 nm by reaction of the cysteine thiol with 5,5′-dithiobis(2-nitrobenzoic acid) using an extinction coefficient of 14150 M^{-1} cm^{-1} (*22*). FTase concentration was determined by absorbance at 280 nm using an extinction coefficient of 150000 M^{-1} cm^{-1} (*23*). FPT inhibitor II (I2) was purchased from Calbiochem-Novabiochem Corp. (San Diego, CA).

Preparation of FTase. Mutagenesis of the FPT/pET23a plasmid was performed using the QuikChange site-directed mutagenesis kit (Stratagene) with the following codon changes: Lys164αAla, AAA to GCA; His248*β*Ala, CAC to GCC; Tyr300*β*Phe, TAC to TCC. The changes were confirmed by DNA sequencing (University of Michigan DNA Sequencing Core). Recombinant rat FTase was overexpressed in *Escherichia coli* BL21(DE3) cells and purified as described previously, with the changes noted below (*24*). The second phenyl column was omitted, and the final phenyl-Sepharose column was run in a 2−0 M KCl gradient. After each column, the protein fractions were tested for FTase activity in a 96-well plate. Each well contained 50 mM Heppso, pH 7.8, 5 mM $MgCl_2$, 1 mM TCEP, 0.2 μM FPP (Sigma), 1 μM Dns-GCVLS, and 10 μL of protein sample (100 μL total volume). The relative fluorescence of each fraction was detected directly after the addition of Dns-GCVLS by the Polarstar Galaxy fluorescence platereader (BMG Lab Technologies, Durham, NC; λ_{ex} = 320 nm, λ_{em} = 520 nm). FTase eluted in two peaks from the final phenyl-Sepharose column, the first peak at 1 M KCl and the second peak at 0 M KCl. Substrate binding studies with Dns-GCVLS demonstrated that the FTase isolated in the first peak has a contaminant bound at the active site (data not shown); therefore, the second peak was used in all studies. The purified FTase was determined by SDS−PAGE to be >90% pure. The protein from peak 2 was dialyzed against HT buffer

(50 mM Hepes, pH 7.8, 1 mM TCEP), concentrated to 40−60 μM, and frozen at −80 °C.

Transient Kinetics. Single turnover assays were performed for FTase mutants K164Aα, H248Aβ, and Y300Fβ at varying magnesium concentration (all mutants) and pH (K164Aα and Y300Fβ) as described previously (*15*). The reaction pH was varied between 5.5 and 9.0 using the following buffers (50 mM): Mes−NaOH (pH 5.5, 6.1), Bes−NaOH (pH 6.5, 7.0), Heppso−NaOH (pH 7.8, 8.0), and Bicine−NaOH (pH 8.3, 9.0). The $MgCl_2$ concentration was varied from 0.01 to 60 mM. The ionic strength in the reactions was kept constant at 0.2 M with the addition of NaCl, and 1 mM TCEP was used as a reductant. Reactions with farnesylation rate constants of less than 0.1 s^{-1} were measured manually using 0.8 μM FTase, 0.4 μM [^{3}H]FPP, and 100 μM GCVLS (8 μL reaction volume). FTase was preincubated with [^{3}H]FPP for 15 min, and then the reaction was initiated by addition of GCVLS. The reactions were quenched at varying times (3 s to 3 h) by the addition of 8 μL of cold 2-propanol and placed on ice. For reactions with product formation rate constants faster than 0.1 s^{-1}, a KinTek rapid quench apparatus was used (KinTek Corp., Austin, TX). The 30 μL reactions contained 0.2 μM FTase, 0.1 μM [^{3}H]FPP, and 100 μM GCVLS. The reactions were quenched with 80% 2-propanol and 20% acetic acid at varying times (0.005 to 600 s), then dried under vacuum, and resuspended in 50% 2-propanol.

The product was separated from substrate by thin-layer chromatography on polyester-backed silica gel plates (Whatman PE SIL G) with an 8:1:1 (v/v/v) 2-propanol/NH_4OH/H_2O mobile phase. The product migrates in this mobile phase, but the FPP substrate remains at the origin, so the plates were cut accordingly and the radioactivity was quantified by scintillation counting. The radioactivity in the product was divided by the total radioactivity for each time point to calculate percent product formed. The rate constant for product formation (k_{obs}) was determined by fitting eq 1 to these data, where P_t is the product formed at time t and P_∞ is the calculated reaction end point, which varied from 65% to 90%.

$$\frac{P_t}{P_\infty} = 1 - e^{-k_{obs}t} \quad (1)$$

The magnesium dependence at each pH was determined by plotting the k_{obs} against the $MgCl_2$ concentration and fitting eq 2 to the data. K_{Mg} represents the apparent dissociation constant, k_{max}^{Mg} is the rate constant of the reaction at saturating magnesium concentration, and k_0 is the rate constant of the reaction in the absence of magnesium. The magnesium-dependent pK_a was determined for the mutants K164Aα and Y300Fβ using a weighted fit of eq 3 to the data, where $K_{1/2}^{Mg}$ is the pH-independent magnesium binding constant.

$$k_{obs} = \frac{k_{max}^{Mg}}{1 + K_{Mg}/[Mg^{2+}]} + k_0 \quad (2)$$

$$K_{Mg}^{app} = K_{1/2}^{Mg}(1 + 10^{pK_a - pH}) \quad (3)$$

Reaction with FMP. The reactions with [^{3}H]FMP were performed at pH 6.1, the optimum pH of the reaction for both wild-type and mutant FTase (*15*) (data not shown). The assays were done as described above for [^{3}H]FPP. The TLC plates were run in a 7:2:1 (v/v/v) 2-propanol/NH_4OH/H_2O mobile phase, and eq 1 was fit to the data.

Peptide Binding Affinity. The pK_a of the peptide substrate thiol was determined as previously described by measuring the affinity of FTase·I2 for dansyl-GCVLS as a function of pH (*11*). The binding of dansyl-GCVLS to FTase was observed by FRET (fluorescence resonance energy transfer), where the tryptophan residues of FTase are excited at 280 nm and the bound dansyl group emits at 496 nm. The samples were prepared with the pH buffers described above (50 mM), 2 mM TCEP, 1 mM $MgCl_2$, 40 nM I2, 20 nM K164Aα or Y300Fβ FTase, and 10 nM EDTA. The ionic strength of the samples was maintained at 0.1 M with NaCl. The sample was preincubated for 15 min, and then aliquots of Dns-GCVLS (0−4 μM) were added with a 2 min stirred and a 1 min unstirred incubation prior to each measurement. A weighted fit of eq 4 to the data at each pH yielded the apparent dissociation constants, where ΔFL represents the observed fluorescence corrected for background, EP is the fluorescence end point, IF is the initial fluorescence, [Pep] is the concentration of Dns-GCVLS, and K_D^{app} is the apparent dissociation constant for Dns-GCVLS. To calculate the thiol pK_a from the pH dependence of Dns-GCVLS binding, the K_D^{app} as a function of pH was fit by eq 5, where K_D is the maximum dissociation constant for Dns-GCVLS, pK_{a1} was set as the pK_a of the free peptide thiol (8.1), and pK_{a2} is the pK_a of the enzyme-bound peptide thiol.

$$\Delta FL = \frac{EP}{1 + K_D^{app}/[Pep]} + IF \quad (4)$$

$$K_D^{app} = \frac{K_D(1 + 10^{pH - pKa_1})}{1 + 10^{pH - pKa_2}} \quad (5)$$

FPP Binding Affinity. FPP dissociation constants were determined by equilibrium dialysis in 50 mM Heppso−NaOH, pH 7.8, 5 mM $MgCl_2$, 5 μM $ZnCl_2$, and 1 mM TCEP as described previously (*13*). One side of the dialysis membrane contained 1 mL of 20 nM [^{3}H]FPP, while the opposite side contained 1 mL of mutant FTase (0−200 nM). After being shaken at 4 °C for 24 h, duplicate aliquots of 100 μL were withdrawn from each chamber and analyzed by liquid scintillation counting. Dissociation constants for FPP, K_D^{FPP}, were calculated using a nonlinear least-squares fit of eq 6 to the data, where [E·FPP] is the concentration of enzyme-bound FPP, $[FPP]_{tot}$ is the total concentration of FPP in the chamber containing FTase, $[E]_{free}$ is the concentration of free enzyme, and EP is the maximal ratio of bound FPP to total FPP.

$$\frac{[E\cdot FPP]}{[FPP]_{tot}} = \frac{EP}{1 + K_D^{FPP}/[E]_{free}} \quad (6)$$

RESULTS

Mutagenesis of the Diphosphate Binding Pocket. To determine the influence of specific amino acids in the diphosphate binding pocket on the farnesylation rate constant, residues K164α, H248β, and Y300β were mutated to remove

Scheme 1

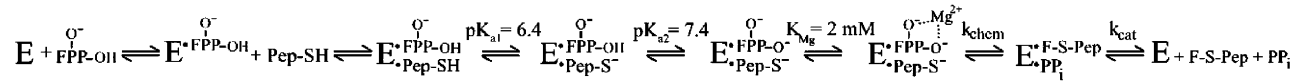

Table 1: Kinetic Constants of FTase Mutants

FTase	k_{max} (s^{-1})[a]	k_0 (s^{-1})[b]	K_D^{FPP} (nM)	K_D^{GCVLS} (nM)[c]	$K_{1/2}^{Mg}$ (mM)	k_{chem}^{FMP} (s^{-1})
wild type	10 ± 1[d]	$(1.6 \pm 0.8) \times 10^{-2}$	6.5 ± 1.7[g]	62 ± 8[e]	2.0 ± 0.2[d]	$(6.8 \pm 0.2) \times 10^{-4}$
K164Aα	0.33 ± 0.01	$(5.7 \pm 0.2) \times 10^{-4}$	2.5 ± 0.7[f]	70 ± 6	2.3 ± 0.1	$(5.6 \pm 0.5) \times 10^{-4}$
H248Aβ	0.99 ± 0.06[h]	$(1.0 \pm 0.1) \times 10^{-3}$	14 ± 2	ND[i]	3.4 ± 0.2[h]	$(1.44 \pm 0.07) \times 10^{-4}$
Y300Fβ	$(1.96 \pm 0.04) \times 10^{-2}$	$(2.0 \pm 0.4) \times 10^{-4}$	20 ± 10	50 ± 8	0.9 ± 0.1	$(2.3 \pm 0.3) \times 10^{-6}$

[a] k_{max} is the pH-independent rate constant for product formation at saturating concentrations of $MgCl_2$. [b] k_0 is the rate constant for product formation in the absence of $MgCl_2$ at pH 7.8. [c] Peptide dissociation constants were measured with Dns-GCVLS at pH 7.6. [d] Data from ref *15*. [e] Data from ref *11*. [f] Data from ref *21*. [g] Data from ref *13*. [h] These values are the constants at pH 7.8, not the pH-independent value. [i] ND denotes not determined.

functionality from their side chains. Lysine 164α and histidine 248β were each changed to alanine (K164Aα, H248Aβ), and tyrosine 300β was changed to a phenylalanine (Y300Fβ). Replacement of His or Lys by Ala changes not only the charge and hydrogen-bonding characteristics of the side chain but also the van der Waals contacts; the volume change for a Lys to Ala mutation is 64.5 Å^3 while the volume change for a His to Ala mutation is 66.4 Å^3 (*25*). The mutant enzymes had expression levels in *E. coli* comparable to those of wild type (30 mg/L cell culture) and behaved similarly to the wild-type enzyme during purification.

Effect of Mutagenesis on Product Formation. To investigate the function of residues in the diphosphate binding pocket, the rate constant for product formation for each of the mutants was determined. For mammalian FTase, k_{cat} and k_{cat}/K_m do not reflect the rate constant of the chemical step; k_{cat}/K_m and k_{cat} mainly reflect the rate constants for substrate association and product dissociation, respectively. We measured the rate constant of the chemical step (k_{chem}) under single turnover conditions where the enzyme concentration is higher than the FPP concentration. The enzyme is preincubated with FPP to form E·FPP, then the reaction is initiated with addition of excess GCVLS to rapidly form the E·FPP·GCVLS ternary complex, and then the rate constant for the formation of farnesylated product is measured (Scheme 1). The farnesylation rate constant measured for the mutants is consistent with previous measurements by pre-steady-state kinetics [Y300Fβ, H248Aβ (*20*)] and transient kinetics [K164Aα (*21*)]. For wild-type FTase, the observed rate constant (k_{obs}) at 1 mM magnesium, pH 7.8, is 1.7 s^{-1} (*15*). Of the mutations, H248Aβ decreases k_{obs} 5-fold (0.3 s^{-1}), K164Aα has a 30-fold decrease (0.06 s^{-1}), and Y300Fβ reduces k_{chem} 170-fold (0.01 s^{-1}) (Figure 1B). However, the mutants cause larger decreases under optimal catalytic conditions. The pH-independent rate constant (k_{max}) at saturating magnesium concentrations is 10 s^{-1} for wild-type FTase (*15*). Of the mutations, H248Aβ decreases k_{max} 10-fold (1 s^{-1}), K164Aα shows a 30-fold decrease (0.3 s^{-1}), and, most dramatically, the Y300Fβ substitution reduces k_{max} 500-fold (0.02 s^{-1}) (Table 1, Figure 1A).

Ligand Binding Affinity. The affinity of the FTase mutants for FPP was measured by equilibrium dialysis. The K_D^{FPP} values of K164Aα, H248Aβ, and Y300Fβ are within 3-fold of the wild-type K_D^{FPP} measured under identical conditions [Table 1 (*26*)]. The binding affinity of mutant FTase for Dns-GCVLS was determined by fluorescence. The K_D^{GCVLS} values for the mutants were also similar to those of wild type at pH 7.8 (Table 1). Therefore, these mutations have little or no effect on substrate binding affinity.

Magnesium Dependence of Catalysis. Due to the proximity of the diphosphate binding residues to the proposed magnesium binding site, the magnesium dependence (K_{Mg}) of k_{chem} was measured for the K164Aα, H248Aβ, and Y300Fβ mutants. Wild-type FTase was previously shown to have a pH-independent $K_{1/2}^{Mg}$ of 2 mM (*15*). At pH 7.8, the magnesium dependence of K164Aα, H248Aβ, and Y300Fβ is unchanged from that of wild type (Figure 1B). Therefore, the effect of these residues on catalysis is independent of magnesium binding.

The observed magnesium affinity constant (K_{Mg}) for wild type decreases as the pH increases with an apparent pK_a of 7.4, which is proposed to reflect deprotonation of the terminal phosphate of FPP (*15*). The tribasic diphosphate coordinates the magnesium ion with higher affinity, and the bound Mg^{2+} facilitates catalysis by stabilizing the developing charge on the nonbridging oxygens in the transition state. The K_{Mg}^{app} was measured as a function of pH for K164Aα and Y300Fβ to determine if these mutations alter the pH dependence of magnesium binding. Previous measurements indicated that these mutations alter the pH dependence of steady-state parameters (*12*, *20*). The magnesium-dependent pK_as observed for K164Aα and Y300Fβ using transient kinetics are similar to those of wild-type FTase, at 7.5 $\pm$ 0.1 and 7.3 $\pm$ 0.1, respectively (Figure 1C, Table 2). The pH-independent magnesium affinity, represented by $K_{1/2}^{Mg}$, is also relatively unchanged from wild type for K164Aα and Y300Fβ (Table 1). Additionally, the farnesylation rate constant of the reaction in the absence of magnesium is dramatically attenuated in these mutants; k_0 is decreased 16-fold for H248Aβ, 28-fold for K164Aα, and 80-fold for Y300Fβ at pH 7.8 (Table 1). These data clearly indicate that these residues do not facilitate magnesium binding, and further they establish that these residues are not involved, either directly or indirectly, in the ionization that enhances Mg^{2+} affinity.

pH Dependence of Peptide Binding. Another ionization that enhances the FTase farnesylation rate constant is the stabilization of the peptide substrate cysteine thiolate upon binding to the active site zinc (*11*, *12*). The coordination of the cysteine sulfur to the zinc ion lowers its apparent pK_a from 8.1 free in solution to 6.4 upon binding to the enzyme.

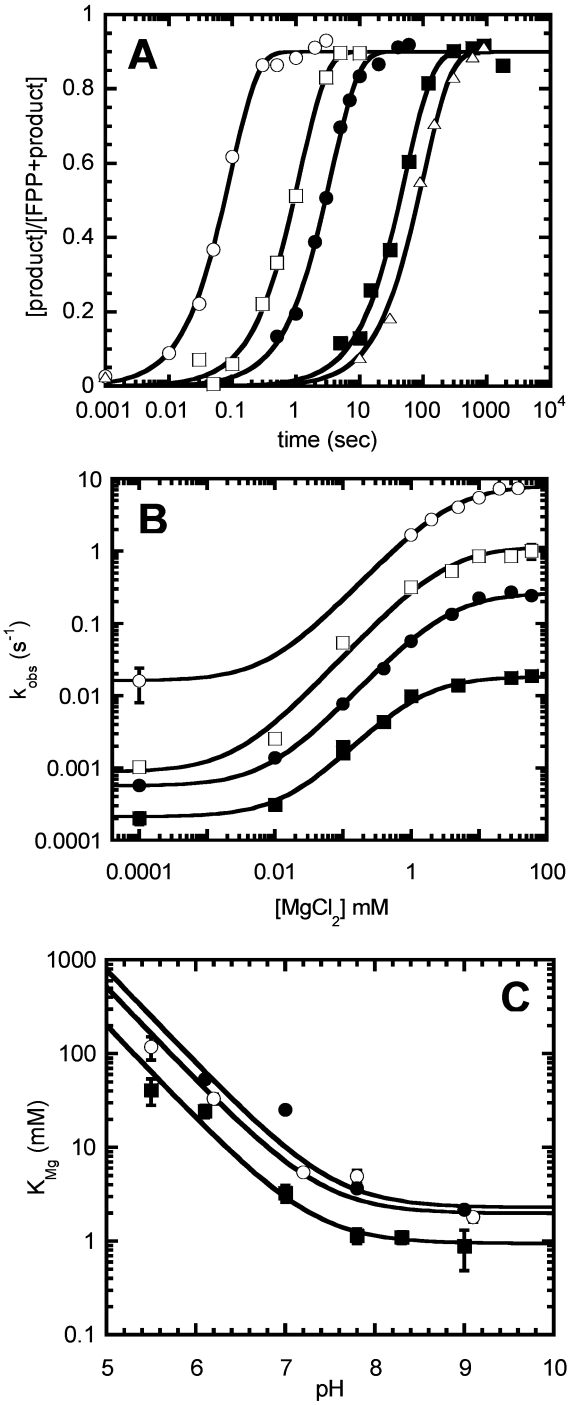

FIGURE 1: Effect of mutations on the magnesium dependence of the FTase reaction. (A) Single turnover assays were conducted as described under Experimental Procedures for wild-type FTase (○), H248A (□), K164A (●), and Y300F (■) at saturating magnesium (10−60 mM $MgCl_2$) and wild-type FTase in the absence of magnesium (△) at pH 7.8. Equation 1 was fit to the data to determine k_{obs} and normalized for clarity using the equation $(CPM_{prod} - CPM_{min})/(CPM_{max} - CPM_{min}) \times 0.9$. (B) Single turnover reactions at varying magnesium (0−60 mM) were performed at pH 7.8 as described under Experimental Procedures for wild-type FTase (○), H248A (□), K164A (●), and Y300F (■), and eq 2 was fit to the data. (C) pH dependence of K_{Mg} for wild-type FTase (○), K164A (●), and Y300F (■), fit by eq 3. Wild-type data were taken from Saderholm et al. (*15*).

To test if K164α and Y300β of FTase alter stabilization of the zinc-bound thiolate, this pK_a was determined by measuring the binding affinity of the dansylated peptide, Dns-GCVLS, for the K164Aα and Y300Fβ mutant enzymes as a function of pH (Figure 2, Table 2). For the Y300Fβ mutant, the pH dependence curve overlays the wild-type curve, and the pK_a is comparable at 6.2 ± 0.1, so the hydroxyl group of this residue must not stabilize the enzyme-bound thiolate or enhance the affinity of the peptide substrate. The K164Aα mutant, however, has an altered pH dependence of peptide binding; the mutant enzyme has a similar affinity for the deprotonated peptide as the wild-type enzyme, but the affinity of the protonated peptide is decreased more than 10-fold in the mutant ($K_D > 10$ μM). The pK_a for the deprotonation of the peptide thiolate bound to K164Aα can be estimated as <5 using a thermodynamic box ($K_{D4} = K_{D1}K_{D3}/K_{D2}$; Scheme 2). From the crystal structures of the ternary complex of FTase (*17*, *18*), it is unclear how Lys164α could directly interact with the substrate thiol to alter the pK_a, since they are not within an appropriate distance to interact. Therefore, it is likely that this lysine stabilizes the binding of the protonated peptide to the enzyme.

Table 2: pH Dependence of FTase Mutants K164Aα and Y300Fβ

FTase	pK_{a1}[a]	pK_{a2}[b]
wild type	6.4 ± 0.1[c]	7.4 ± 0.1[d]
K164Aα	<5	7.5 ± 0.1
Y300Fβ	6.2 ± 0.1	7.3 ± 0.1

[a] pK_{a1} was determined from the pH dependence of Dns-GCVLS binding to FTase·I2. [b] pK_{a2} was determined from the pH dependence of K_{Mg}. [c] Data from ref *11*. [d] Data from ref *15*.

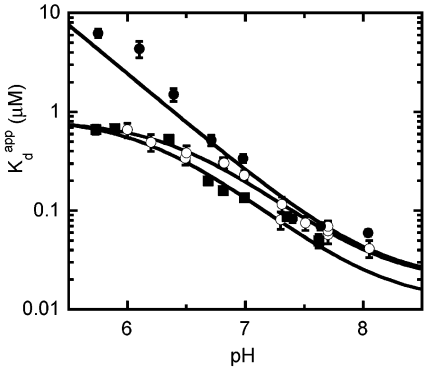

FIGURE 2: pH dependence of peptide binding to wild-type FTase (○), K164A (●), and Y300F (■). The K_D^{app} of Dns-GCVLS binding to the enzyme was measured at varying pH (5.7−8.1) by fluorescence as described under Experimental Procedures, and eq 5 was fit to the data. Wild-type data were from Hightower et al. (*11*).

Scheme 2

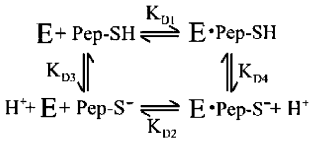

Reactivity with FMP. Mutations at residues K164α and Y300β significantly decrease the chemical rate constant but do not affect the magnesium-dependent pK_a, the dependence of the reaction on magnesium, or the affinity of substrates for the enzyme. The Y300Fβ mutation also does not affect the thiol pK_a, yet decreases the rate constant for product formation by 500-fold. To further investigate the function of these residues, we compared the transient kinetics for product formation using FMP compared to FPP as a

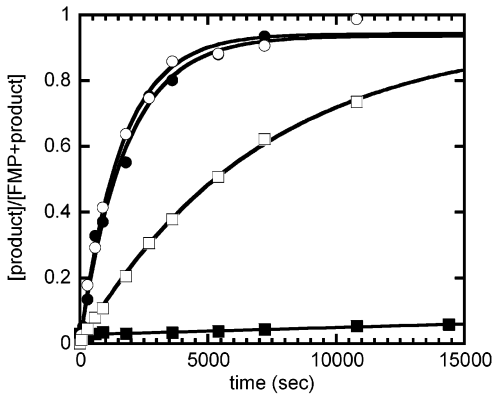

FIGURE 3: Single turnover kinetics of wild-type and mutant FTase with FMP. Wild-type FTase (○), H248A (□), K164A (●), and Y300F (■) were incubated with [^{3}H]FMP and reacted with GCVLS as described under Experimental Procedures. Equation 1 was fit to the data to determine k_{obs} and normalized for clarity using the equation $(CPM_{prod} - CPM_{min})/(CPM_{max} - CPM_{min}) \times 0.9$.

substrate. The reaction of wild-type FTase with FMP is independent of magnesium concentration and demonstrates a pH dependence curve with two pK_as of ~5.5 (*15*). At pH 6.1, near the maximal k_{chem}^{FMP}, the farnesylation rate constant for wild-type FTase is $(7 \pm 1) \times 10^{-4}$ s^{-1}. The crystal structures (*17*) of the E·FPP and inactive ternary complexes indicate that K164α interacts with the α-phosphate of FPP and that H248*β* and Y300*β* interact with the *β*-phosphate of FPP. Therefore, we predicted that only mutation of K164α would affect the rate constant of catalysis using FMP as a substrate. Surprisingly, however, we observed the opposite results when we examined the three mutant enzymes. The rate constant of the chemical step using FMP is virtually unaffected by the K164Aα mutation (5.6×10^{-4} s^{-1}) but is decreased 300-fold in the Y300F*β* mutant (2.3×10^{-6} s^{-1}) and 5-fold in the H248A*β* mutant (1.4×10^{-4} s^{-1}) (Figure 3). These differences are almost certainly not due to a change in mechanism for the two mutants, as the pH dependence of the farnesylation rate constant with the FMP substrate is not affected (data not shown). These data demonstrate that Y300*β* and, to a lesser extent, H248*β*, but not K164α, stabilize the transition state relative to the E·FMP·peptide complex. This result suggests that Y300*β* and H248*β* interact with the phosphate of FMP and, by analogy, the α-phosphate of FPP in the normal reaction catalyzed by FTase.

DISCUSSION

General Acid−Base Catalysis. The polar amino acids around the FPP binding pocket are highly conserved among the prenyltransferases FTase and GGTase I, yet the role of these residues is still not well understood. The k_{chem} values determined by the single turnover studies of the mutants K164Aα, H248A*β*, and Y300F*β* agree with previously published pre-steady-state data and, in particular, indicate that the hydroxyl group of Tyr300*β* is very important for enhancement of farnesylation catalyzed by FTase. Wu and colleagues and Rozema and Poulter (*12*, *20*) have suggested that Tyr300*β* and Lys164α act as acid−base catalysts of farnesylation for mammalian and yeast FTase, respectively. These studies showed a change in the pH dependence of the steady-state kinetic constants for the mutant enzymes. However, these apparent pK_as determined from the pH dependence of steady-state turnover do not necessarily directly reflect changes in thermodynamic ionizations since product and substrate dissociation is slow relative to the farnesylation step (*27*, *28*).

Under single turnover conditions that directly measure the chemical step, our data show that the mutation of K164α and Y300*β* has no effect on the magnesium-dependent pK_a of mammalian FTase, a property that likely reflects ionization of the diphosphate leaving group. Additionally, the pH dependence of peptide binding to the mutant enzymes shows that the pK_a of the enzyme-bound peptide thiol of the Y300F*β* mutant is also unchanged from the wild-type value. Therefore, there are no data indicating that Y300*β* acts as a general acid−base to catalyze farnesylation in FTase. The K164Aα mutant, however, does show a decrease in the enzyme-bound peptide thiol pK_a relative to wild type. The high K_D values at low pH compared with the normal K_D values at high pH suggest that the K164Aα enzyme has a very low affinity for the thiol peptide (PepSH) but can bind the thiolate peptide ($PepS^-$) with identical affinity as the wild type. Mutation of lysine to alanine removes the positive charge, the hydrogen bond donating ability, and also deletes the van der Waals volume from this position in the active site. The positive charge on Lys164α was noted to be important for peptide binding in previous studies (*21*). In the crystal structure of the FTase ternary complex with the isoprenoid analogue I2 and a K-Ras peptide, Lys164α is 3.25 Å from the backbone carbonyl oxygen of the peptide residue on the N-terminal side of the cysteine (TKCVIM) (*16*; Figure 4). It is possible that when the bound peptide is protonated, the zinc−thiol bond lengthens, allowing a hydrogen bond between Lys164α and the backbone carbonyl to form and enhance the affinity of the protonated peptide.

Magnesium Affinity. The farnesylation rate constants of mutants K164Aα, H248A*β*, and Y300F*β* are accelerated in the presence of magnesium by 460-, 1200-, and 90-fold, respectively, at pH 7.8, paralleling the 500-fold acceleration observed with wild type at this pH. The magnesium dependence of k_{chem}, represented by K_{Mg}, is unchanged for the mutants relative to wild-type FTase. Therefore, these residues are not important for binding magnesium. Crystal structures of the FTase ternary complex containing the FPP analogue I2 cocrystallized with Mn (in place of magnesium) proposed that Lys164α moves to allow for metal binding; however, our data indicate that removal of the Lys side chain does not alter the apparent magnesium affinity, suggesting that the movement observed in the crystal structure has no observed energetic consequences.

Computer calculations on the FTase·FPP binary complex have predicted that the interactions between the negatively charged diphosphate and the positively charged residues of the diphosphate binding pocket are the principal source of binding energy for FPP (*29*). However, this report and others show that eliminating the positive charge of one of the diphosphate binding pocket amino acids through mutagenesis has only a modest effect (3-fold or less) on the K_D of FPP binding to the enzyme (*21*, *26*). Consistent with this, FPP·Mg^{2+} binds with a similar affinity to the enzyme as FPP, suggesting that the negative charge on the diphosphate moiety is not the dominant factor for FPP affinity for FTase (*13*).

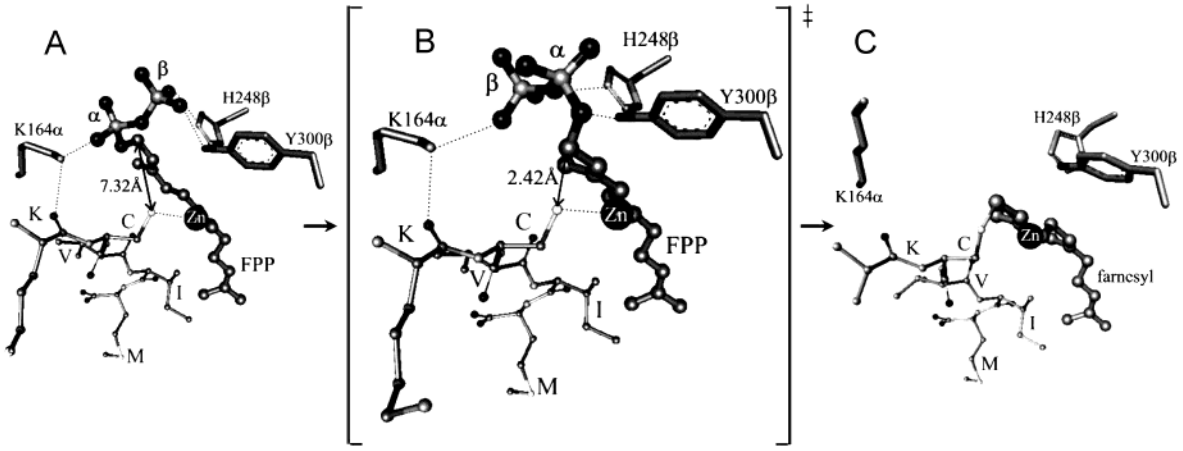

FIGURE 4: Computational model of the proposed active substrate conformation. (A) Model of the inactive FTase·FPP·KCVIM ternary complex, where the C1 of FPP and the peptide thiolate are separated by 7.32 Å. The complex was created by overlaying the two crystal structures FTase·FPP·L-739750 [PDB ID 1JCQ (*17*)] and FTase·I2·K-Ras peptide [PDB ID 1D8D (*16*)] in MOE to 1.8 Å RMSD and then creating a FTase·FPP·K-Ras peptide by deleting one of the FTase molecules, L-739750, and I2 from the overlay. The sequence N-terminal of KCVIM in the K-Ras peptide was omitted for clarity. (B) Proposed active substrate conformation of FTase, which brings the C1 of FPP within reacting distance of the peptide thiolate. The bond angles of FPP were adjusted using MOE to reflect an active conformation consistent with the diphosphate rearrangement predicted by the kinetic data presented here. (C) Crystal structure of the FTase·product complex. The coordinates of the side chain of the farnesyl-KCVIM lysine beyond C_β were absent from the PDB and, thus, are not shown.

Conformation of FPP. FTase has also been structurally well characterized by crystallographic studies. However, the crystal structures of the ternary complex all reflect an inactive FPP binding mode where the two reacting atoms, the C1 of FPP and the cysteine thiolate, are greater than 7 Å apart, presumably due to the fact that the complexes are formed with components that are catalytically inactive (*16*−*18*). The recent crystal structure of the FTase·product complex suggests that, in the catalytically competent ternary complex, the conformation of the FPP molecule is altered where the first and second prenyl units are rotated so that the C1 of FPP is close to the zinc-bound sulfur (*19*). These rotations likely also affect the position of the diphosphate moiety bound to FTase. To examine the location of the bound diphosphate in the active complex, we have measured the effects of mutations on the farnesylation transition state using FMP compared to FPP as a substrate. Assuming that the FMP molecule binds in the same way and proceeds through the transition state of the FTase reaction in the same way as FPP, the single phosphate of FMP models the α-phosphate of FPP. Surprisingly, these studies demonstrate that removal of the hydroxyl of Tyr300*β* affects the reactivity of both FPP and FMP equally, suggesting that this group interacts with the α-phosphate of FPP. Similarly, the data suggest that H248*β* interacts with the α-phosphate, although more weakly. In contrast, the K164Aα mutation only affects the reactivity of FPP, suggesting that this side chain interacts with the *β*-phosphate of FPP to stabilize the transition state. One reasonable explanation for these data is that the position of the diphosphate moiety changes from that in the inactive ternary complex visualized in the crystal structure to an active substrate conformation like the one presented in Figure 4. For the purposes of this discussion, this conformation will be referred to as an active substrate conformation, which is a distinct ES complex from that studied crystallographically. However, our data cannot delineate between a substrate conformation present only in the transition state versus an intermediate active ES complex representing an energy minimum along the reaction coordinate prior to the transition state.

Given that the FTase·product crystal structure demonstrates that the first and second prenyl groups rearrange relative to the binding pocket to bring C1 of FPP within reacting distance of the thiolate of the peptide, it is reasonable to hypothesize that the position of the diphosphate moiety adopts an altered conformation as well. After rotation of the first two isoprene units of FPP so that the two reacting atoms, C1 and the peptide thiolate, are less than 2.5 Å apart, the diphosphate can be positioned such that the phosphate oxygen bound to C1 of FPP is within hydrogen-bonding distance of Y300*β*. This places the diphosphate bridging oxygen in position to interact with H248*β* and the *β*-phosphate within hydrogen-bonding distance of K164α. This altered substrate conformation may be important for setting up interactions that maximally stabilize the development of negative charge on the diphosphate predicted by the "exploded" transition state (*13*, *14*). The synergy between the conformational change of bound FPP and peptide binding is likely a method the enzyme uses to limit catalysis of hydrolysis of FPP in the absence of peptide or to prevent reaction with other nonspecific substrates, thus optimizing the specific farnesylation reaction. The importance of the presence of the peptide chain is evidenced by the fact that the farnesylation rate constant of the E·FPP·peptide complex is enhanced 10^3-fold compared to the reaction with small thiols, such as dithiothreitol and 2-mercaptoethanol, with similar pK_as (*30*). Other enzymes, such as hexokinase, use conformational changes to alter the rates of reaction with a substrate nucleophile compared to H_2O, although in these cases the conformational change is mainly in the protein and not in the substrate (*31*).

Taken together, the data suggest that the dramatic chemical rate attenuation resulting from mutation of Tyr300*β* is due to the absence of a critical hydrogen bond that energetically stabilizes the "active" FPP conformation relative to the "inactive" conformation. A 500-fold decrease in the enzyme-catalyzed rate constant of farnesylation upon deletion of the

tyrosine hydroxyl corresponds to destabilization of the transition state by 15.4 kJ/mol, which is consistent with the energy of a charged hydrogen bond (*32*). A hydrogen bond between the hydroxyl group of Tyr300β and the α-phosphate of FPP could also stabilize the transition state in this reaction by stabilizing the developing negative charge on the leaving group (diphosphate or phosphate).

These studies provide key insight into the structure of the transition state of FTase, which has been elusive to crystallographic analysis. FTase inhibitor studies can benefit from this model by creating transition state mimics to tightly bind to the enzyme active site. Further mutagenesis studies in the diphosphate binding pocket coupled with a computational analysis of FPP binding modes will test our model of the ground and transition state structure and add more detail to our understanding of the FTase reaction.

ACKNOWLEDGMENT

The authors thank Carolyn Weinbaum for technical assistance and Chris Holley for preliminary characterization of the H248Aβ mutant.

REFERENCES

1. Zhang, F. L., and Casey, P. J. (1996) *Annu. Rev. Biochem. 65*, 241−269.
2. Casey, P. J., Solski, P. A., Der, C. J., and Buss, J. E. (1989) *Proc. Natl. Acad. Sci. U.S.A. 86*, 8323−8327.
3. Schafer, W. R., Kim, R., Sterne, R., Thorner, J., Kim, S. H., and Rine, J. (1989) *Science 245*, 379−385.
4. Hancock, J. F., Magee, A. I., Childs, J. E., and Marshall, C. J. (1989) *Cell 57*, 1167−1177.
5. Figueroa, C., Taylor, J., and Vojtek, A. B. (2001) *J. Biol. Chem. 276*, 28219−28225.
6. Cox, A. D. (2001) *Drugs 61*, 723−732.
7. Sebti, S. M., and Hamilton, A. D., Eds. (2001) *Farnesyltransferase Inhibitors in Cancer Therapy*, Humana Press, Totowa, NJ.
8. Reiss, Y., Brown, M. S., and Goldstein, J. L. (1992) *J. Biol. Chem. 267*, 6403−6408.
9. Chen, W. J., Moomaw, J. F., Overton, L., Kost, T. A., and Casey, P. J. (1993) *J. Biol. Chem. 268*, 9675−9680.
10. Huang, C.-c., Casey, P. J., and Fierke, C. A. (1997) *J. Biol. Chem. 272*, 20−23.
11. Hightower, K. E., Huang, C.-c., Casey, P. J., and Fierke, C. A. (1998) *Biochemistry 37*, 15555−15562.
12. Rozema, D. B., and Poulter, C. D. (1999) *Biochemistry 38*, 13138−13146.
13. Huang, C., Hightower, K. E., and Fierke, C. A. (2000) *Biochemistry 39*, 2593−2602.
14. Dolence, J. M., and Poulter, C. D. (1995) *Proc. Natl. Acad. Sci. U.S.A. 92*, 5008−5011.
15. Saderholm, M. J., Hightower, K. E., and Fierke, C. A. (2000) *Biochemistry 39*, 12398−12405.
16. Long, S. P., Casey, P. J., and Beese, L. S. (2000) *Structure 8*, 209−222.
17. Long, S. B., Hancock, P. J., Kral, A. M., Hellinga, H. W., and Beese, L. S. (2001) *Proc. Natl. Acad. Sci. U.S.A. 98*, 12948−12953.
18. Strickland, C. L., Windsor, W. T., Syto, R., Wang, L., Bond, R., Wu, Z., Schwartz, J., Le, H. V., Beese, L. S., and Weber, P. C. (1998) *Biochemistry 37*, 16601−16611.
19. Long, S. B., Casey, P. J., and Beese, L. S. (2002) *Nature 419*, 645−650.
20. Wu, Z., Demma, M., Strickland, C. L., Radisky, E. S., Poulter, C. D., Le, H. V., and Windsor, W. T. (1999) *Biochemistry 38*, 11239.
21. Hightower, K. E., De, S., Weinbaum, C., Spence, R. A., and Casey, P. J. (2001) *Biochem. J. 360*, 625−631.
22. Riddles, P. W., Blakeley, R. L., and Zerner, B. (1979) *Anal. Biochem. 94*, 75−81.
23. Wu, Z., Demma, M., Strickland, C. L., Syto, R., Le, H. V., Windsor, W. T., and Weber, P. C. (1999) *Protein Eng. 12*, 341−348.
24. Zimmerman, K. A., Scholten, J. D., Huang, C.-c., Fierke, C. A., and Hupe, D. J. (1998) *Protein Expression Purif. 14*, 395−402.
25. Rellick, L. M., and Becktel, W. J. (1997) *Biopolymers 42*, 191−202.
26. Kral, A. M., Diehl, R. E., deSolms, S. J., Williams, T. M., Kohl, N. E., and Omer, C. A. (1997) *J. Biol. Chem. 272*, 27319−27323.
27. Furfine, E. S., Leban, J. J., Landavazo, A., Moomaw, J. F., and Casey, P. J. (1995) *Biochemistry 34*, 6857−6862.
28. Cleland, W. W. (1982) *Methods Enzymol. 87*, 390−405.
29. Chehade, K. A., Kiegiel, K., Isaacs, R. J., Pickett, J. S., Bowers, K. E., Fierke, C. A., Andres, D. A., and Spielmann, H. P. (2002) *J. Am. Chem. Soc. 124*, 8206−8219.
30. Hightower, K. E., Casey, P. J., and Fierke, C. A. (2001) *Biochemistry 40*, 1002−1010.
31. Bennett, W. S., Jr., and Steitz, T. A. (1978) *Proc. Natl. Acad. Sci. U.S.A. 75*, 4848−4852.
32. Fersht, A. R. (1987) *Biochemistry 26*, 8031−8037.

BI0346852